Available online at www.sciencedirect.com
ScienceDirect
International Journal of Mass Spectrometry 262 (2007) 256–262
International Journal of Mass Spectrometry
www.elsevier.com/locate/ijms

Spatially dynamic laser patterning using advanced optics for imaging matrix assisted laser desorption/ionization (MALDI) mass spectrometry

Stacy D. Sherrod, Edward T. Castellana, John A. McLean [1], David H. Russell *

Laboratory for Biological Mass Spectrometry, Department of Chemistry, Texas A&M University, College Station, TX 77843-3255, USA

Received 17 November 2006; received in revised form 30 November 2006; accepted 4 December 2006
Available online 11 January 2007

Abstract

Beam homogenization and spatially dynamic beam patterning optics have been combined to improve the imaging matrix assisted laser desorption/ionization time of flight mass spectrometry (MALDI–TOFMS) experiment. The optical design was developed to improve upon the spatial resolution limit imposed by the laser beam profile (~25–50 μm) and to decrease the long analysis times associated with mechanical translation of the MALDI sample stage. This arrangement consists of: laser beam conditioning optics, laser beam shaping optics via a digital micromirror device (DMD), and an imaging lens system. Experimental results comparing traditional imaging MALDI–TOFMS and spatially dynamic imaging MALDI–TOFMS are discussed. The optical system has proven useful for patterning the MALDI laser beam into user defined beam shapes, can potentially decrease analysis times associated with mechanical movement of the sample stage, and may be capable of increasing the limits of detection by simultaneously irradiating multiple spots.

Keywords: MALDI; Imaging mass spectrometry; Laser optics; Digital micromirror device

1. Introduction

Imaging mass spectrometry (MS) utilizing secondary ion mass spectrometry (SIMS) [1,2], laser microprobe mass spectrometry (LMMS) [3,4], matrix assisted laser desorption/ionization (MALDI) [5–7], and desorption electrospray ionization (DESI) [8] offers the ability to simultaneously obtain spatial and chemical information of analytes on a wide variety of surfaces, such as inorganic, organic and biologically relevant substrates. Recent reports underscore the importance of imaging MS for the spatial profiling of biomolecules (e.g., proteins, peptides) in pathologically relevant tissue [9–12]. Also, the ability to combine histopathology with spatial expression profiles of disease specific biomarkers [13,14] has the potential for disease diagnosis, prognosis, and to assist in selecting patient specific treatment strategies [14].

Early imaging MS experiments were performed using SIMS [1,2] and LMMS [3,4]. Whereas SIMS offers near unparallel spatial resolution, its application to bioimaging is limited by the low ionization efficiencies for high mass ions (molecular weights >1000 Da). Although some progress has been made to enhance signal for high mass ions using matrix enhanced (ME) SIMS [15], nanoparticle (Au or Ag) incorporated SIMS [16], and thin metal (Au) layer ME-SIMS [17], large biomolecules (i.e., proteins) cannot be ionized as intact species. The first successful application of imaging mass spectrometry for analyzing high mass proteins dates back to the late 1990s, when Caprioli and colleagues reported the ability to directly image peptides and proteins in thin (~10–20 μm) tissue sections using MALDI–TOFMS [5]. After obtaining mass spectra for peptides/proteins (mass range of 500–~25,000 Da) [18] at each spatial location, individual spectra were reconstructed to generate molecular ion images of specifically chosen biomolecules.

Although significant advances in sample preparation and data processing have been made, the instrumental arrangement used for imaging MALDI–TOFMS applications has not changed significantly. For example, conventional optics consist of an aperture and a single focusing lens, thus the spatial resolution (size of laser beam at sample surface) is dictated by the diffraction limit of the optical system as well as the shape of the laser

* Corresponding author. Tel.: +1 979 845 3345; fax: +1 979 845 9485.
E-mail address: russell@mail.chem.tamu.edu (D.H. Russell).
[1] Current address: Department of Chemistry and Vanderbilt Institute of Chemical Biology, Vanderbilt University, Nashville, TN, USA.

1387-3806/$ – see front matter © 2006 Elsevier B.V. All rights reserved.
doi:10.1016/j.ijms.2006.12.003

beam. The diffraction limit of an optical system can be estimated by:

$$D = \frac{1.22\lambda}{\mathrm{NA}} \quad (1)$$

where D is the diffraction limited diameter, λ the wavelength of light, and NA the numerical aperture [19]. Under our current instrumental constraints (NA of 0.05) the diffraction limit of a N_2 laser (337 nm) is about 8 μm. The maximum spatial resolution obtainable for a particular imaging MALDI–TOFMS system is determined by the laser spot size (diffraction limited) and the precision of the sample plate micropositioners; typical spatial resolutions range between 25 and 50 μm. Several strategies have been investigated to increase spatial resolution in imaging MS [5,7,20–26]. Specifically, placing a static aperture in front of the focusing lens system has been successfully employed to decrease the laser spot size in imaging MALDI–TOFMS [5,23]. Scanning microprobe MALDI [20] and near-field scanning optical microscopy (NSOM) coupled with MALDI [21,22] have also been used to further decrease the laser spot size to the submicron range. All of these techniques suffer from a decreased sensitivity for high mass ions since fewer analytes are sampled in a smaller area [26] and fragmentation increases owing to the high laser fluences that are required [27,28]. In practice, however, the maximum achievable spatial resolution is limited by the overall amount of sample present in individual irradiation volumes. As irradiation volumes become infinitely small the sample concentration approaches zero. Thus, limits in spatial resolution ultimately arise from instrumental constraints such as ionization efficiency and limits of detection. Other investigators have improved the spatial resolution in imaging MS by using techniques such as oversampling [24], a parallel sample preparation using glass beads [29], or special ion optics incorporating a position-sensitive detector (known as the ion microscope) [7,26].

Even with these recent advances, current imaging MALDI–TOFMS techniques suffer from static beam shape and long analysis times (minutes to hours) due to the slow mechanical movement of the MALDI plate and low repetition rate lasers typically used in MALDI experiments (e.g., 3–30 Hz). Furthermore, ion image quality should be improved by using square pixels (square beam dimensions) rather than conventional circular pixels (circular beam dimensions). The spatially dynamic optical system described herein provides significant improvements for the imaging MS experiment and consists of: (i) the primary MALDI laser beam, (ii) beam conditioning optics, (iii) a digital micromirror device (DMD), and (iv) an imaging lens system [30,31]. DMDs have found widespread application in video imaging, projection, and telecommunications, but analytical chemistry applications of these devices are limited [32], thus far restricted to spectroscopy applications [33–36] and microarray fabrication [37,38].

2. Experimental methods

Imaging MALDI–TOFMS experiments were performed on a Voyager DE-STR (Applied Biosystems, Foster City, CA) instrument under optimized conditions in linear mode. This instrument utilizes a nitrogen laser (337 nm), where the laser spot is elliptical, with dimensions of ~50 μm × 90 μm. Crystal violet, hexamethyl-pararosanaline (Sigma–Aldrich, St. Louis, MO), was deposited onto a nitrocellulose membrane sheet (Bio-Rad Laboratories, Hercules, CA) in the shape of an ampersand "&." The crystal violet solution was prepared at 20 mg/mL in methanol/H_2O (95/5, v/v). The nitrocellulose membrane was then attached directly to a stainless steel MALDI plate using double sided conducting tape (SPI supplies, West Chester, PA).

Peptides (human angiotensin I and II, DRVYIHPFHL (M_r = 1295.68) and DRVYIHPF (M_r = 1045.54), respectively) were used without further purification (American Peptide, Vista, CA). The peptide solutions were prepared at 1 mg/mL in H_2O. α-cyano-4-hydroxycinnamic acid (CHCA) (Sigma–Aldrich, St. Louis, MO) was re-crystallized in ethanol and washed with diethyl ether prior to use. A 10 mg/mL solution of CHCA was prepared in 60/40 acetonitrile/water containing 0.1% trifluoroacetic acid, v/v. Samples were prepared by mixing both peptide/matrix 1/1, v/v, followed by spotting a 1 μL mixture onto the MALDI plate. For peptide microarray studies, peptides were spotted onto a MALDI plate using a computer controlled microspotter (ProBot, LC Packings, Sunnyville, CA).

The beam conditioning optics were evaluated using a nitrogen laser (337 nm, Spectra Physics, Inc., Mountain View, CA) and a CCD camera (Spiricon, Inc., Logan, UT). Images were captured from a screen placed after various components in the optical path. Data were acquired for the unconditioned, expanded, and expanded and homogenized beam.

Spatially dynamic imaging experiments were also performed on a Voyager DE-STR instrument under optimized conditions in both linear and reflected mode utilizing a Nd:YAG laser (355 nm, Tempest-20, New Wave Research, Inc., Fremont, CA). Fig. 1 shows a diagram of the optical imaging setup. The laser beam is first split into two distinct paths using a 355 nm beamsplitter (CVI laser, Inc., Albuquerque, NM). 70% of the original beam (imaging beam path) follows the spatially dynamic optical imaging route, while the remaining 30% follows the non-imaging route. The imaging beam path was expanded 3× using a beam expander (CVI laser, Inc., Albuquerque, NM) coated with an antireflective coating for 355 nm. Following expansion, beam homogenization was performed using two microlens arrays (Süss MicroOptics, Neuchâtel, Switzerland) in series, and beam shaping is achieved using a digital micromirror device (DMD) (Tyrex Services Group, Ltd., Austin, Texas). Each microlens array consists of two crossed-cylindrical lens arrays of 300 μm pitch. The DMD consists of 1024 × 768 (~1×10^6) individual mirror elements having dimensions of 13 μm per side. Light reflecting from the DMD was focused onto the sample plate using an imaging lens system which consists of two different lenses (UV grade fused silica, Optosigma, Santa Ana, CA). The focal lengths of both lens 1 and 2 were 39.3″ and 6″, respectively.

The intensity of the non-imaging beam was attenuated by a 1/2 waveplate and polarizing beamsplitter cube (CVI laser, Inc., Albuquerque, NM). The beam is temporally aligned using a variable beam path stage and four 355 nm mirrors (CVI laser, Inc., Albuquerque, NM). Following temporal alignment, two

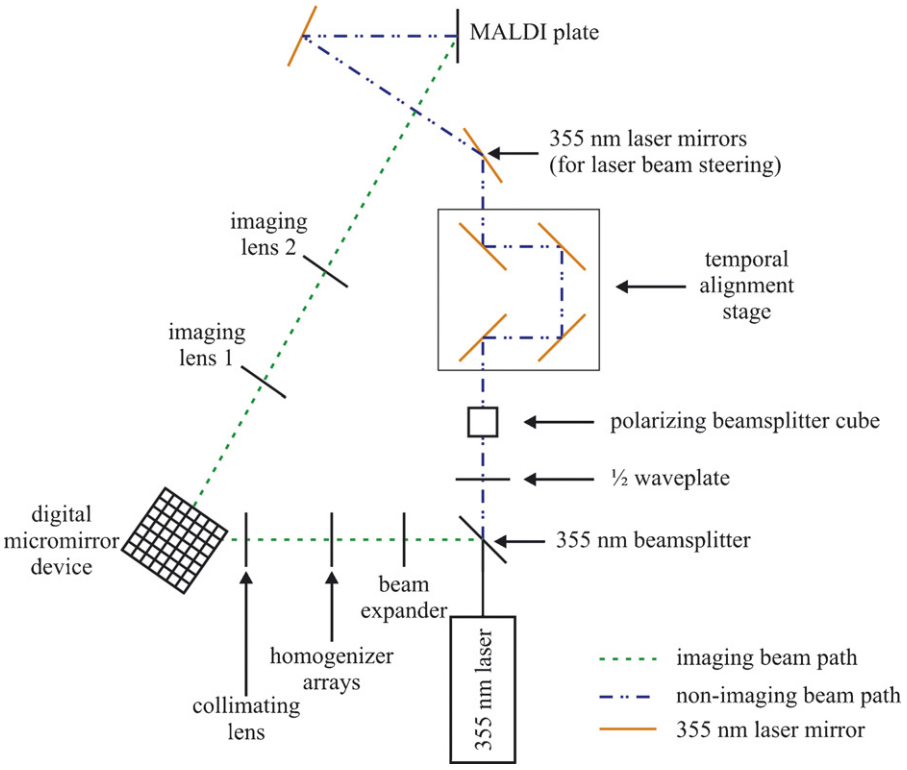

Fig. 1. Diagram of the optical imaging system used in these studies. The laser beam is split into two directions, the imaging path (blue dotted line) and non-imaging beam path (green dotted-dashed line). (For interpretation of the references to color in this figure legend, the reader is referred to the web version of the article.)

additional 355 nm mirrors were used to direct the beam to the MALDI plate.

3. Results and discussion

There are several significant instrumental challenges associated with acquiring imaging data using the static beam positioning scheme: (i) poor spatial resolution owing to the MALDI laser spot size (ca. 25–50 μm), (ii) fixed laser shape, (iii) inability to probe the spacing between neighboring laser irradiations, (iv) current mechanical repositioning schemes, which are slow and have limited spatial precision, and (v) analysis times directly proportional to the number of spatial elements (*x*–*y* coordinates). The spatially dynamic laser patterning optical arrangement described herein has the potential to address each of these challenges.

The general principle of imaging MALDI–TOFMS is illustrated in Fig. 2. The spatial distribution for an organic dye (*m*/*z* 372) was obtained by rastering the laser spot across the sample while recording a TOF mass spectrum at each coordinate. The information contained at each coordinate is shown in Fig. 2C. If multiple analytes are present in the sample, different ion images can be acquired by interrogating the data set for each analytes corresponding mass-to-charge ratio (*m*/*z*).

We have designed a spatially dynamic optical arrangement to improve imaging MALDI–TOFMS experiments (Fig. 3A). This optical arrangement allows for beam expansion, homogenization, collimation, shaping, and imaging. First, the primary MALDI laser beam (Fig. 3B, i) is expanded and directed through two cross-cylindrical homogenizer arrays. The purpose of these homogenizer arrays is to produce a flat-top beam profile (uniform intensity distribution, Fig. 3B, ii). This flat-top beam profile is accomplished by splitting the primary laser beam into wavelets that diverge, overlap, and mix with one another. By using two homogenizer arrays in series, the beam is divided into $\sim 8.1 \times 10^5$ wavelets, which when superimposed produce a flat-top wavefront. Beam homogenization minimizes differences in laser fluence at the sample target which translates to increased reproducibility of MS ion signals [39]. Homogenization also insures that the data acquired in a spatially resolved format is obtained under comparable conditions. In that, all coordinates in an image will be analyzed at the same fluence (absence of laser hot spots).

Laser beam profiles obtained at three different regions in the optical train (unconditioned, expanded, and expanded and homogenized) is illustrated in Fig. 4. Note that the primary and expanded laser beam profiles (Fig. 4A and B) contain hot spots, which are observable as distinct peaks in the line profiles. The laser beam profile following beam expansion and homogenization illustrates the reduction of hot spots (Fig. 4C), because the line profiles (in both the *x* and *y* dimension) are approaching a flat-top profile. The beam conditioning optics (specifically the homogenizers) are very efficient for conditioning Gaussian profile beams into flat-top profile beams. Because the Nd:YAG used in our experiments has a Gaussian profile beam we decided to demonstrate a worse case condition, i.e., nitrogen laser (irregular profile beam) to illustrate the effects of beam conditioning. Even though the homogenizers may not produce a true flat-top profile

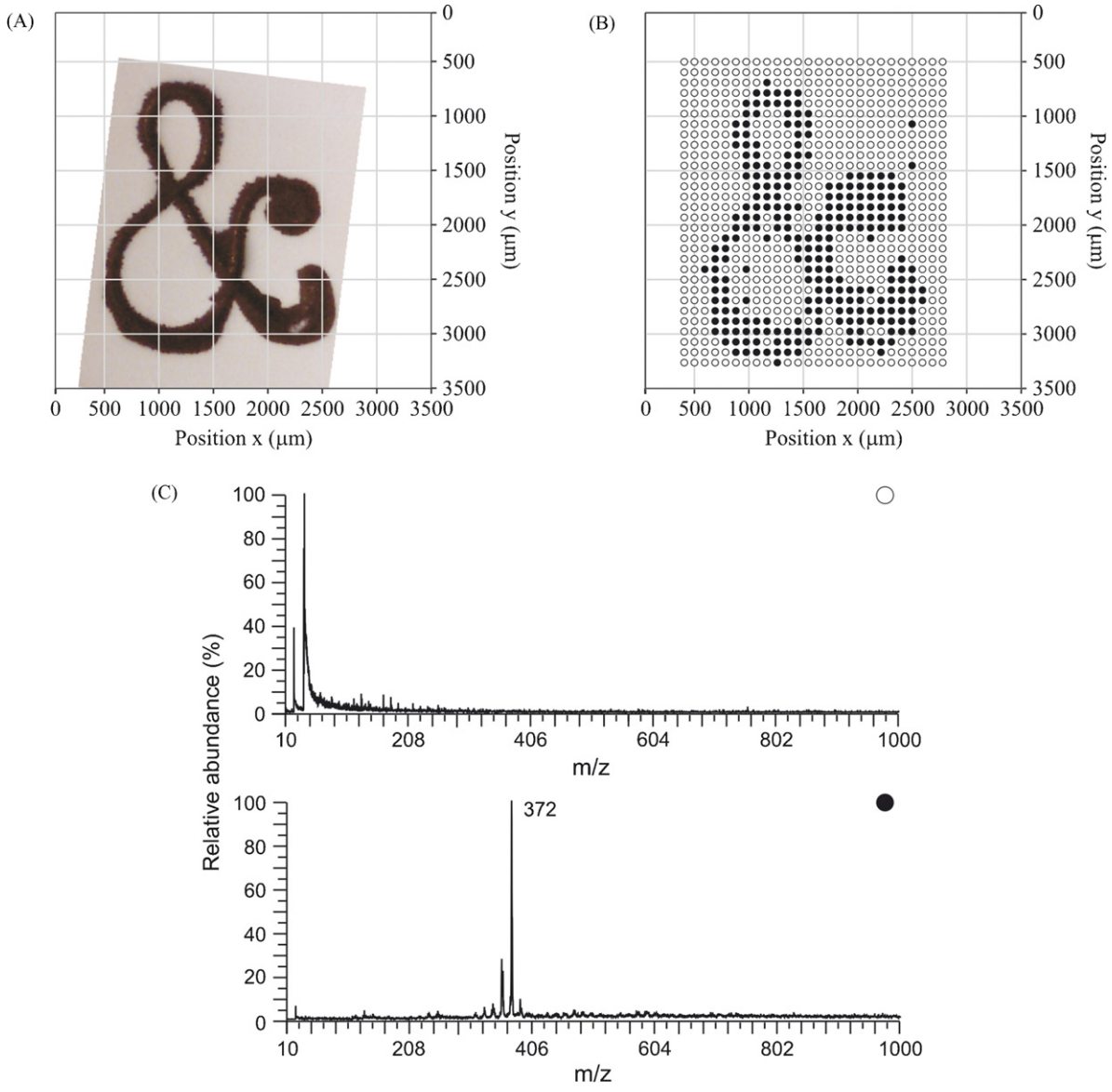

Fig. 2. Ion image of crystal violet (*m/z* 372) deposited onto nitrocellulose. (A) Optical microscopy image of the deposited material. (B) Corresponding image obtained by LDI–TOFMS where open and closed circles represent mass spectra with a signal-to-noise ratio less than and greater than 10 at *m/z* 372, respectively. (C) Representative mass spectra for open (top) and closed circles (bottom) in the ion image shown in (A). Each mass spectrum represents the average of 10 laser shots and the laser spot (ellipse, ca. 50 μm × 90 μm) was translated in 95 μm increments to produce the resulting 780 pixel image. (For interpretation of the references to color in this figure legend, the reader is referred to the web version of the article.)

it is possible to select certain portions of the line profiles to be used in the experiment owing to downstream optical components. For example, only the flat-top portion (and not the wings) of the beam can be selected to be imaged onto the MALDI plate.

After beam homogenization, the laser beam is collimated with a lens and projected onto a digital micromirror device (DMD) (Fig. 3A). Each mirror in the DMD is individually addressed by loading a pattern onto on-board memory, which can be quickly changed (up to 5 kHz) in a predetermined and/or dynamic sequence. Based on the bi-stable state of each mirror, the projected MALDI irradiation is the pattern of reflected light from the DMD. An example of light patterning is shown in Fig. 3B, iii, which contains digital photographs of light patterned as the letters "IJMS". This illustrates our ability to easily pattern the MALDI laser into regular shapes (e.g., round, square, rectangular, etc.) or into complex shapes with variable dimensions. Furthermore, the ability to irradiate multiple mirrors at the same time on the DMD allows tailored non-congruent targeted spatial regions to be irradiated simultaneously.

The imaging lens system is used to form a demagnified image of patterned light onto the sample stage. This lens design utilizes a pair of UV lenses in series, where the lens spacing and focal lengths are chosen to optimize both demagnification and numerical aperture given the instrumental constraints (Fig. 3A). That is, the MALDI instrument source housing used in these experiments limits the patterned light to be demagnified by 0.44, this demagnification does not supply the necessary energy (fluence < 1 μJ/cm^2) needed to generate ions by MALDI.

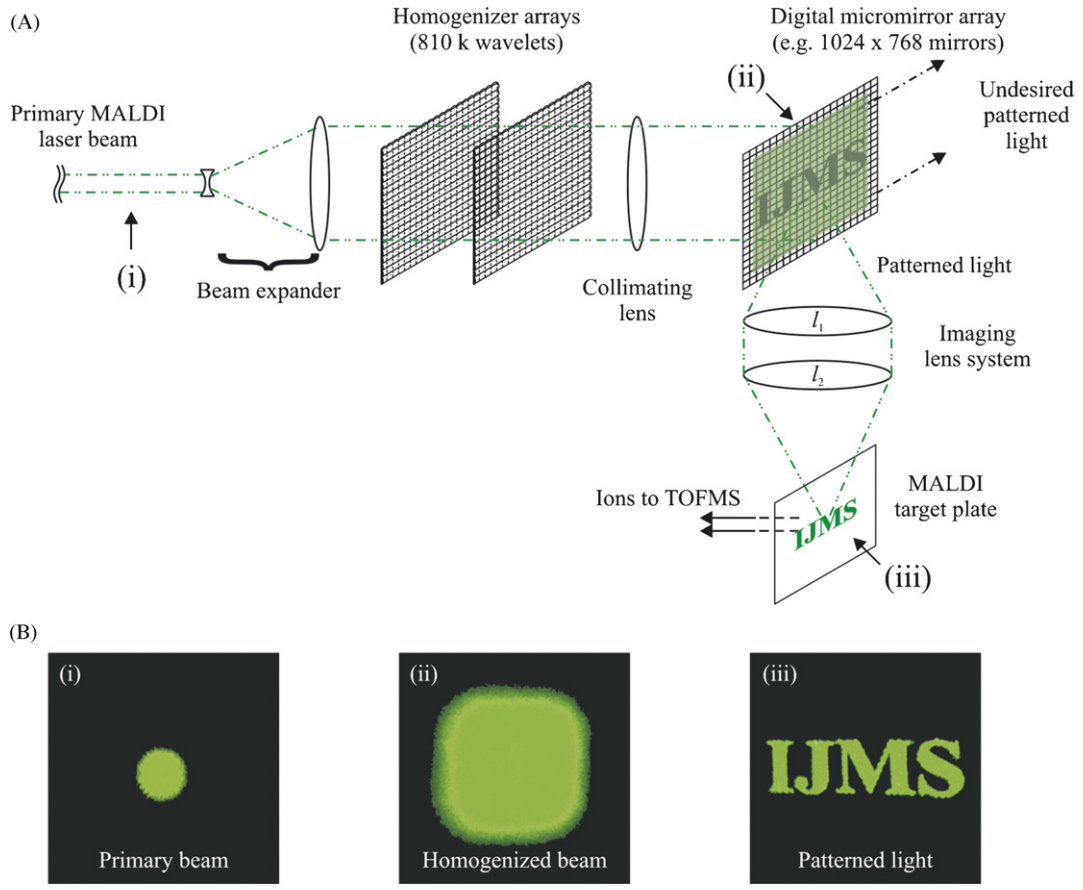

Fig. 3. (A) Schematic diagram of the MALDI optics used for spatially dynamic optical imaging mass spectrometry. (B) Digital photographs illustrating the light profile obtained in different regions of the optical arrangement in (A). Photographs of the (i) primary beam, (ii) expanded and homogenized beam and (iii) pattern beam imaged onto the target stage.

Proof-of-concept experiments were performed using a split laser beam set-up, whereby the laser beam is split into two different paths (see Fig. 1). A portion (70%) of the laser beam is directed toward the imaging optical train which allows beam conditioning and shaping, and another portion (30%) of the beam is directed toward the MALDI plate by a series of mirrors (see Section 2 for specific details). Both beams were temporally aligned so that both irradiate the MALDI plate at the same time. The non-imaging beam irradiates the entire viewable area of the MALDI plate, and is attenuated just below threshold fluence for MALDI. Fig. 5A contains a mass spectrum obtained by irradiating the sample with light from the non-imaging beam path. A similar spectrum (i.e., no ion signal) is obtained if the sample is irradiated by only the imaging beam path. However, when the

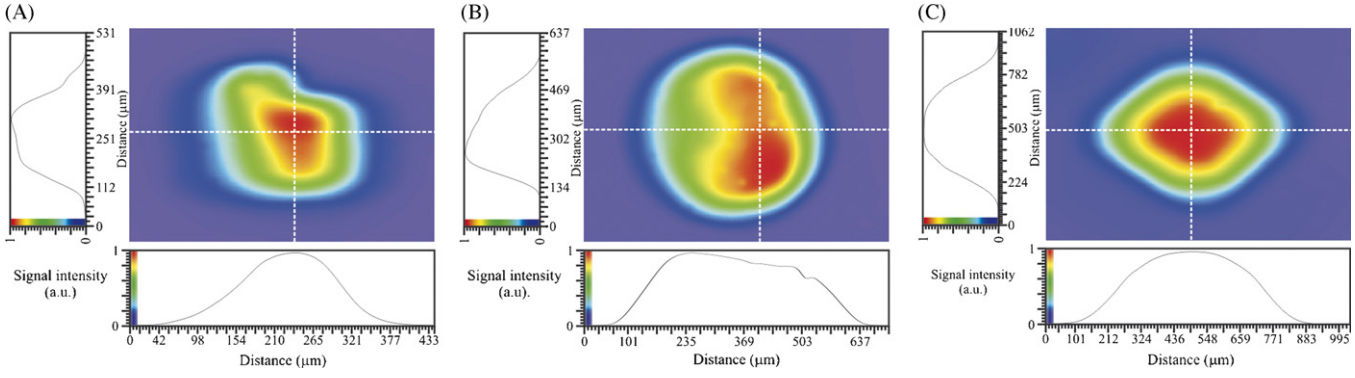

Fig. 4. Laser beam output profiles illustrating beam profiles at several different regions of the optical setup. (A) Hot spots in the output beam intensity profile of a primary N_2 laser are evident (beam dimensions of ~300 μm × 400 μm). (B) Laser beam profile following beam expansion also shows hot spots within the laser and increases the beam dimensions to ~600 μm × 425 μm. (C) Laser beam profile following beam expansion and homogenization (beam dimensions of ~800 μm × 800 μm). The primary N_2 laser beam has been transformed into a more flat-top profile beam (left and bottom). The white dotted lines represent signal intensity beam profiles in the *y* and *x* dimensions, respectively. Each plot is an average of 16 laser shots.

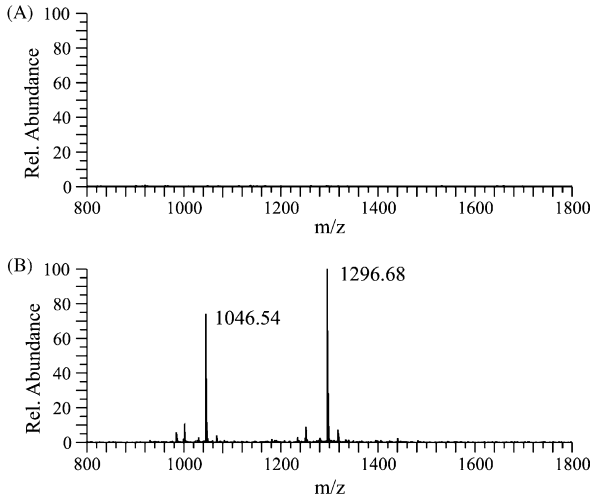

Fig. 5. Mass spectra obtained by using the optical imaging system (A) with the non-imaging beam path only and (B) with both beam paths open. Each mass spectrum represents the average of 500 laser shots (reflected mode) and the uploaded image on the DMD is chosen to be a square of 90 × 90 mirrors where the position of light is in the center of the viewable area.

sample is irradiated by light from both beam paths, strong signal for the two analytes angiotensin I and II ($[M+H]^+$) are observed (Fig. 5B).

Imaging MS is illustrated by using the split laser beam setup to interrogate a 2 × 2 peptide microarray of angiotensin I and II (Fig. 6). For these experiments, the laser beam was patterned using the DMD to irradiate individual spots in the array, without mechanically moving the MALDI sample stage. Fig. 6A contains the mass spectra for angiotensin II from spots irradiated by the non-imaging beam (top) and with both imaging and non-imaging beams (bottom). When both imaging and non-imaging beam paths are open, signals for the $[M+H]^+$ ion (*m/z* 1047.2) are observed. The same results are illustrated in Fig. 6B for angiotensin I (*m/z* 1297.5). Operating the instrument in reflected mode was investigated as a means of obtaining high-resolution spectra, however laser position proved to be important; laser sampling significantly off the TOF axis yielded little to no ion detection. Subsequently, all spectra in these experiments were acquired in linear mode to decrease dependence on laser position.

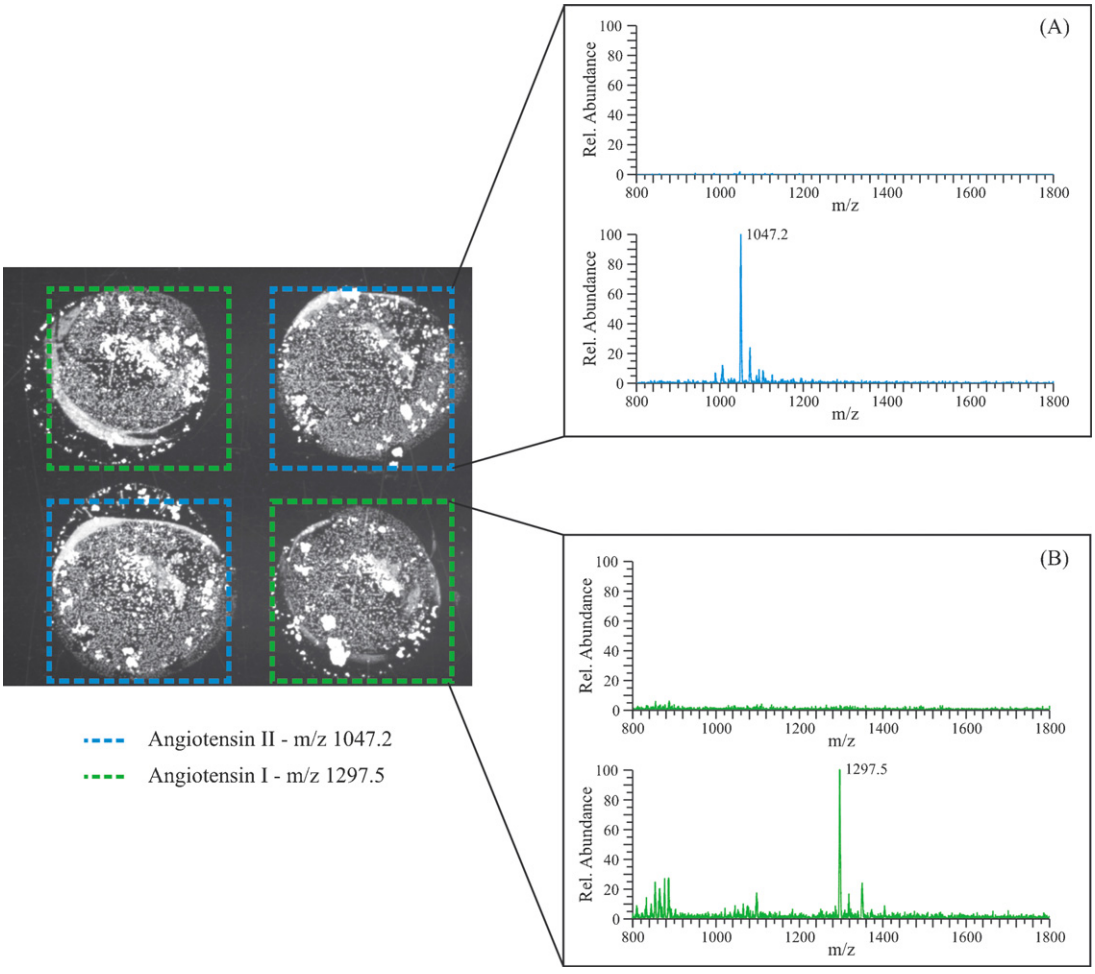

Fig. 6. Optical microscopy image of a 2 × 2 peptide microarray deposited on a MALDI plate, where colored boxes (green and blue, corresponding to 750 μm × 750 μm) represent areas containing angiotensin I and II, respectively. (A and B) Mass spectra obtained by using the spatially dynamic optical imaging system (A and B, top) with the non-imaging beam only and (A and B, bottom) with both imaging and non-imaging beams. Each mass spectrum represents the average of 250 laser shots (linear mode), where the uploaded image (90 × 90 mirrors) on the DMD is changed to irradiate the desired spot. (For interpretation of the references to color in this figure legend, the reader is referred to the web version of the article.)

4. Conclusions

In this study, we demonstrate the ability to perform imaging MS using a spatially dynamic optical arrangement. The imaging experiments described differ from traditional imaging MS experiments in that user defined laser beam shape and dimension can be chosen to improve image quality. Patterning light also alleviates the inability to probe the areas between laser irradiations (spaces between laser spots). In principle, it is feasible to increase throughput using this optical arrangement because the DMD allows for faster laser spot relocation relative to sample stage movement.

Clearly, numerous molecular imaging applications are amenable to laser patterning optics. For example, this technique could be used for MALDI–TOFMS imaging of tissue samples, where the advantage of this approach is that imaging could be performed by irradiating single or multiple cells simultaneously. Advanced algorithms could then be implemented for rapid data analysis to compare differences in the mass spectra for the identification of differential expressions. This type of experiment is analogous to a molecular specific, on-line laser capture microdissection imaging experiment in that it allows for an intelligent interrogation of cells.

We are currently developing an imaging lens system to increase demagnification and numerical aperture of the imaging beam in an effort to eliminate the need for split beam experiments and to increase the spatial resolution to the sub-micron range (hundreds of nm regime). Also, the limitation imposed by probing samples approaching infinitely small volumes may be addressed by implementing congruent imaging, which allows the simultaneous irradiation of multiple spots at various locations on the sample. Irradiation of visually identical regions (i.e., diseased regions of a tissue sample) which are too small to allow interrogation individually can be simultaneous analyzed. In addition, we plan to incorporate high repetition rate lasers to perform faster analysis and increase sample throughput.

Acknowledgements

Financial support for this work was provided by the National Science Foundation (CHE-9629966) and by the Department of Energy, Division of Chemical Sciences BES (DE-FG03-95ER14505).

References

[1] M.L. Pacholski, N. Winograd, Chem. Rev. 99 (1999) 2977.
[2] R. Castaing, G. Slodzian, J. Microsc. 1 (1962) 395.
[3] L. Van Vaeck, H. Struyf, W. Van Roy, F. Adams, Mass Spectrom. Rev. 13 (1994) 189.
[4] L. Van Vaeck, H. Struyf, W. Van Roy, F. Adams, Mass Spectrom. Rev. 13 (1994) 209.
[5] R.M. Caprioli, T.B. Farmer, J. Gile, Anal. Chem. 69 (1997) 4751.
[6] L. Li, R.W. Garden, J.V. Sweedler, Trends Biotechnol. 18 (2000) 151.
[7] S.L. Luxembourg, T.H. Mize, L.A. McDonnell, R.M.A. Heeren, Anal. Chem. 76 (2004) 5339.
[8] J.M. Wiseman, D.R. Ifa, Q. Song, R.G. Cooks, Angew. Chem., Int. Ed. 45 (2006) 7188.
[9] K. Yanagisawa, Y. Shyr, B.J. Xu, P.P. Massion, P.H. Larsen, B.C. White, J.R. Roberts, M. Edgerton, A. Gonzalez, S. Nadaf, J.H. Moore, R.M. Caprioli, D.P. Carbone, Lancet 362 (2003) 433.
[10] P. Chaurand, R.M. Caprioli, Electrophoresis 23 (2002) 3125.
[11] T.C. Rohner, D. Staab, M. Stoeckli, Mech. Ageing Dev. 126 (2005) 177.
[12] P. Chaurand, S.A. Schwartz, R.M. Caprioli, Curr. Opin. Chem. Biol. 6 (2002) 676.
[13] P. Chaurand, S.A. Schwartz, D. Billheimer, B.J. Xu, A. Crecelius, R.M. Caprioli, Anal. Chem. 76 (2004) 1145.
[14] P. Chaurand, M.E. Sanders, R.A. Jensen, R.M. Caprioli, Am. J. Pathol. 165 (2004) 1057.
[15] A.F.M. Altelaar, J. vanMinnen, C.R. Jimenez, R.M.A. Heeren, S.R. Piersma, Anal. Chem. 77 (2005) 735.
[16] A. Marcus, N. Winograd, Anal. Chem. 78 (2006) 141.
[17] A.F.M. Altelaar, I. Klinkert, K. Jalink, R.P.J. deLange, R.A.H. Adan, R.M.A. Heeren, S.R. Piersma, Anal. Chem. 78 (2006) 734.
[18] R.M. Caprioli, Cancer Res. 65 (2005) 10642.
[19] W.J. Smith, in: R.E. Fischer, W.J. Smith (Eds.), Practical Optical System Layout and Use of Stock Lenses, McGraw-Hill Companies, Inc., New York, 1997, p. 117.
[20] B. Spengler, M. Hubert, J. Am. Soc. Mass Spectrom. 13 (2002) 735.
[21] D.A. Kossakovski, S.D. O'Connor, M. Widmer, J.D. Baldeschwieler, J.L. Beauchamp, Ultramicroscopy 71 (1998) 111.
[22] E. Betzig, J.K. Trautman, T.D. Harris, J.S. Weiner, R.L. Kostelak, Science 251 (1991) 1468.
[23] R.W. Garden, J.V. Sweedler, Anal. Chem. 72 (2000) 30.
[24] J.C. Jurchen, S.S. Rubakhin, J.V. Sweedler, J. Am. Soc. Mass Spectrom. 16 (2005) 1654.
[25] R. Stockle, P. Setz, V. Deckert, T. Lippert, A. Wokaun, R. Zenobi, Anal. Chem. 73 (2001) 1399.
[26] L.A. McDonnell, S.R. Piersma, M.A.F. Altelaar, T.H. Mize, S.L. Luxembourg, P.D.E.M. Verhaert, J. van Minnen, R.M.A. Heeren, J. Mass Spectrom. 40 (2005) 160.
[27] R. Knochenmuss, J. Mass Spectrom. 37 (2002) 867.
[28] K. Dreisewerd, M. Schurenberg, M. Karas, F. Hillenkamp, Int. J. Mass Spectrom. Ion Processes 141 (1995) 127.
[29] E.B. Monroe, J.C. Jurchen, B.A. Koszczuk, J.L. Losh, S.S. Rubakhin, J.V. Sweedler, Anal. Chem. 78 (2006) 6826–6832.
[30] J.A. McLean, D.H. Russell, US Serial No. 11/056,852 (Publication No. 20050242277), Advanced Optics for Rapidly Patterned Laser Profiles in Analytical Mass Spectrometry, 2005.
[31] J.A. McLean, D.H. Russell, International WO2005US004576 (Publication No. WO2005079360), Advanced Optics for Rapidly Patterned Laser Profiles in Analytical Spectrometry, 2005.
[32] D. Dudley, W. Duncan, J. Slaughter, White Paper DLP Products New Applications, Texas Instruments, Inc. Plano, TX 75086.
[33] E.P. Wagner, B.W. Smith, S. Madden, J.D. Winefordner, M. Mignardi, Appl. Spectrosc. 49 (1995) 1715.
[34] R.A. DeVerse, R.M. Hammaker, W.G. Fateley, Vib. Spectrosc. 19 (1999) 177.
[35] W.G. Fateley, R.M. Hammaker, R.A. DeVerse, J. Mol. Struct. 550–551 (2000) 117.
[36] R.A. DeVerse, R.M. Hammaker, W.G. Fateley, Appl. Spectrosc. 54 (2000) 1751.
[37] S. Singh-Gasson, R.D. Green, Y. Yue, C. Nelson, F. Blattner, M.R. Sussman, F. Cerrina, Nat. Biotechnol. 17 (1999) 974.
[38] M. Schena, Microarray Analysis, first ed., Hoboken, New Jersey, 2003.
[39] R.J. Wenzel, K.A. Prather, Rapid Commun. Mass Spectrom. 18 (2004) 1525.